White Rose
university consortium
Universities of Leeds, Sheffield & York

eprints@whiterose.ac.uk
https://eprints.whiterose.ac.uk/

A workflow for modelling fluvial meander-belt successions: combining forward stratigraphic modelling and multi-point geostatistics

Jose M. Montero[1,*], Luca Colombera[1], Na Yan[1] and Nigel P. Mountney[1]

1 – Fluvial & Eolian Research Group, School of Earth and Environment, University of Leeds, Leeds, LS2 9JT, UK

*) Corresponding author. Email: eejmm@leeds.ac.uk

ABSTRACT

A new workflow has been developed for modelling reservoir successions that comprise fluvial meander-belt deposits, based on algorithms that employ multi-point statistics (MPS). A library of training images – from which MPS modelling algorithms can borrow geological patterns for modelling fluvial meandering systems – has been built. The training images incorporate sedimentary architectures relating to point-bar deposits accumulated by fluvial meander-bend expansion and translation, as observed in high-sinuosity river systems and their preserved deposits in the geologic record. The training-image library has been developed using a forward stratigraphic modelling software (PB-SAND) that simulates fluvial meander-bend evolution and resulting point-bar facies organization, and which has been constrained using sedimentological data from geological analogues.

The training images are applied to two widely employed MPS modelling algorithms: SNESIM and DEESSE. Solutions to common issues encountered in MPS modelling workflows have been established through optimization of modelling settings for SNESIM and DEESSE. Auxiliary variables are used to simulate common facies trends. Application of the training-image library through the developed workflows for SNESIM and DEESSE has been tested; the sensitivity of unconditional simulation results to input parameters has been analysed to define modelling recipes, consisting of sets of appropriate modelling parameters for use with each training image and modelling algorithm. The creation of fluvial reservoir models that are geologically realistic using MPS algorithms remains challenging, but the proposed approach holds promise.

Keywords: facies modelling, multi-point statistics, SNESIM, DEESSE, training image, meandering fluvial system

1. INTRODUCTION

Static models depicting the sedimentary architecture of subsurface successions are required to visualize the possible distribution of different properties associated with the rock volume being characterized, to determine volumetric capacities, and for well and production planning (Ringrose and Bentley, 2015). Facies models are used to depict the distribution and the geometry of rock types and constitute the framework on which petrophysical parameters are populated in a digital three-dimensional grid (Caers, 2005; Cannon, 2018; Honarkhah et al., 2010). Facies models simplify lithological heterogeneity, but nevertheless provide a reasonable framework with which to model flow properties (Harding et al., 2004; Walker et al., 1979). To address the considerable uncertainty regarding properties of the bulk reservoir volume, including uncertainty associated with geological heterogeneities at multiple scales, stochastic modelling methods are routinely employed (Ma, 2019; Caers, 2001). Several classes of stochastic methods exist for facies modelling: variogram-based methods (i.e., based on two-point statistics), object-based methods, and methods based on multi-point statistics (MPS) (Pyrcz and Deutsch, 2014; Pyrcz et al., 2008).

Since the 1980s, geomodellers have relied preferentially on variogram- and object-based methods to model different depositional environments, using indicator variograms and Boolean objects, respectively (Guardiano and Srivastava, 1993). However, techniques based on two-point statistics are not especially effective at capturing and reproducing complex geological patterns, such as curvilinear shapes (Journel, 1993; Strebelle, 2000; Strebelle and Journel, 2001). By contrast, object-based methods do permit the reproduction of bodies with complex shapes, but commonly are unable to honour conditioning well data, particularly for densely drilled reservoirs (Deutsch et al., 1996). Techniques based on multi-point statistics (MPS) allow reproduction of complex geological patterns while simultaneously honouring well data, but require suitable and realistic training images to be used as simplified digital representations of the heterogeneities of a reservoir rock (Strebelle and Journel, 2001). A library of suitable training images should, ideally, incorporate stationary features, i.e., patterns that are homogeneous, repeated and not confined to specific locations in the grid. However, the geological bodies that training images seek to model are inherently non-stationary, because the properties of rock types are variable in space (Caers and Zhang, 2004). To enable the reproduction of geological non-stationarity through the application of stationary training images, MPS modelling algorithms employ auxiliary variables that describe how geological properties should vary in space; this permits the incorporation of geological trends in the modelling grids (Chugunova at al., 2008).

A workflow that incorporates an MPS approach, a library of training images constructed using analogue data and forward stratigraphic modelling, and the use of auxiliary variable maps has here been developed to support the construction of facies models for a common type of hydrocarbon reservoirs: high-sinuosity meandering fluvial successions. These facies models incorporate geological features that are commonly difficult to reproduce with traditional subsurface modelling workflows. The application

of training images has been optimized for two MPS algorithms: SNESIM (Strebelle, 2002) and DEESSE (Mariethoz et al., 2010); these algorithms are adopted in this work because they are widely used in the hydrocarbon industry, thanks to their availability in commercial software. For the construction of the training images, a stratigraphic forward modelling approach to simulating geological complexity in meandering fluvial systems and their accumulated successions has been employed (Yan et al., 2017), constrained with data from a wide range of known geological analogues (Colombera et al., 2012a, b).

The aim of this study is to develop and employ a workflow for the generation of unconditional reservoir models that capture the complex lithological heterogeneity inherent in meandering fluvial reservoir successions at multiple scales (Fig. 1). Primary research objectives are as follows: (i) creation of a library of training images that incorporate the main sedimentological and stratigraphic features of meandering fluvial systems and their accumulated deposits; (ii) demonstration of how the training images included in the library can be constrained in terms of their geological realism through the use of data from many known examples stored in a relational database, and of how suitable examples can be selected from the library according to the specifications of different geomodelling cases; (iii) development of an efficient modelling workflow whereby appropriate training images are selected from the library and used to undertake MPS-based simulations.
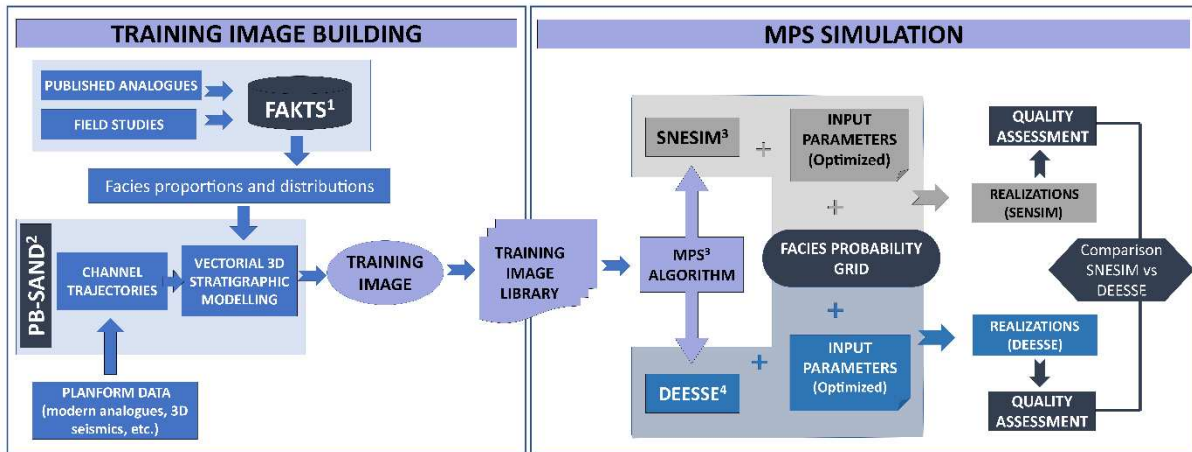
1: FAKTS: Colombera et al. 2012a, b. 2: PB-SAND: Yan et al. (2017). 3: SNESIM: Strebelle and Journel (2000). 4: DEESSE: Mariethoz et al. (2010)

Figure 1. Workflow describing the process for building a training-image library for MPS facies simulations and its application to two different MPS algorithms. The workflow consists of two stages: (i) the creation of training images and (ii) their application to SNESIM (Single Normal Equation SIMulation) and DEESSE (DS, Direct Sampling) (Strebelle, 2002; Mariethoz et al., 2010). The left-hand side of the workflow demonstrates how the training images are built through a novel approach for the synthesis of geological knowledge of the sedimentary architecture of successions deposited by meandering fluvial systems, by using a forward stratigraphic model (PB-SAND) (Yan et al., 2017) constrained using analogue data from a sedimentological database (FAKTS) (Colombera et al., 2012a, b). The box on the right-hand side summarizes the application of the training images for MPS modelling, as undertaken in this work, utilizing input parameters and facies-probability grids that are optimized for the reproduction of features of reservoir architecture typical of meandering fluvial systems. As part of this work, assessment of algorithm outputs and comparisons between realizations of SNESIM and DEESSE are also undertaken.

2. BACKGROUND: MPS MODELLING AND TRAINING IMAGES

Geomodellers commonly rely on pixel-oriented facies-modelling tools based on two-point statistics, which are constrained on indicator variogram models that describe the spatial continuity of the modelling categories ('facies') (Deutsch and Journel, 1998). However, the variogram is merely a measure of continuity, and does not capture significant geological characteristics, such as shape, facies transitions and connectivity (Caers and Zhang, 2004). This is especially problematic, for example, when modelling sinuous channelized bodies. Object-based algorithms are also popular within the geomodelling community. They build geological realizations by placing 3D objects with specific geometries (e.g., ellipsoids, crescents, channels) onto the simulation grid (Bridge and Leeder, 1979; Haldorsen and Damsleth, 1990; Omre, 1991). Object-based methods successfully render the complex geometries of geobodies that are common in fluvial, deltaic and turbiditic successions. However, it may be difficult or impossible to condition the models to subsurface data, particularly in cases where these data are densely distributed, as in the case of seismic surveys or dense well arrays (Ringrose and Bentley, 2015).

By contrast, geomodelling methods based on multiple-point statistics (MPS), which are pixel-based, capture textures by considering more than two points (cells) simultaneously, allowing the reproduction of complex, non-linear spatial correlation (Strebelle and Journel 2000). Overall, the MPS approach combines the strengths of other pixel-based methods (i.e., perfect conditioning to subsurface data) and of object-based methods (i.e., the ability to reproduce complex geological shapes) (Guardiano and Srivastava, 1993; Liu et al, 2005) making them suitable to model fluvial systems with sinuous channels and belts.

Following early attempts at using stochastic methods based on MPS in the geosciences (Farmer, 1988; Deutsch 1992; Xu, 1996), Guardiano and Srivastava (1993) first proposed a direct (non-iterative) MPS algorithm for stochastic simulations. Initial incarnations of MPS modelling algorithms were highly demanding on CPU time, and this issue significantly limited the use of the method. However, Strebelle and Journel (2000) implemented the efficient SNESIM (Single Normal Equation SIMulation) algorithm, which rendered the approach practical by significantly decreasing computer resource requirement. Other MPS algorithms have been created since, including DEESSE (Mariethoz et al., 2010) and IMPALA (Straubhaar et al., 2013). In this study, both SNESIM and DEESSE are used in the devised modelling workflows.

2.1. MPS and training images

A type of input required by MPS algorithms is the so-called 'training image' (TI), which can be defined as a 2D or 3D cellular model acting as a digital representation of the geological architecture of the reservoir interval that needs to be modelled. Therefore, a TI includes the perceived heterogeneity of the geological media, incorporating the geometries, connectivity, spatial distribution and relationships of

geobodies (Journel and Zhang, 2006). Training images can be built using satellite images of modern analogues, idealized models representing the fundamental architectural features of a particular depositional system, or outputs of object-based modelling algorithms or forward stratigraphic models; this last approach has been taken in this work, as explained below.

An MPS algorithm scans a TI to draw patterns that it then replicates across a modelling grid. Once a statistical pattern is acquired from the TI, the MPS algorithm assigns conditional probability distributions of the random variables performing a multi-point analysis of the grid. Training images should ideally honour requirements of stationarity so that patterns can be readily reproduced by MPS modelling algorithms. To meet the assumption of stationarity, TIs are required to have the following attributes: (i) that spatial patterns are reasonably homogeneous over the entire TI (Maharaja, 2008); (ii) that patterns should be repeated throughout the volume or area of the TI; (iii) that sedimentological features in the form of facies and their properties should ideally not be confined to specific locations within parts of a TI, but should instead be distributed throughout the TI grid (Meerschman et al., 2013).

Dealing with geological non-stationarity is one of the main issues faced by geomodellers who employ MPS methods for facies modelling. Since most geological processes in nature result in non-stationary patterns or distributions, the creation and application of suitable TIs is one of the main factors that limit the uptake of MPS modelling algorithms for purposes of subsurface modelling. Because of the stationarity requirements of MPS modelling algorithms, complex geological trends are not readily reproducible in the resulting reservoir models. To enable the reproduction of realistic stratigraphic architectures, MPS modelling inputs include various types of secondary data (auxiliary variables) that can be employed to reproduce spatial trends (Remy et al., 2009; Straubhaar et al., 2011).

MPS methods might be well suited to modelling reservoirs hosted in fluvial successions that represent the product of high-sinuosity river systems, as they allow reproducing complex morphologies such as those of the deposits of meandering rivers (e.g., point bars, channel fills). However, MPS reservoir modelling usually requires extensive effort on model set-up through a 'trial-and-error' approach, whereby the geomodeller performs several simulations to optimize the input parameters with consideration of the outputs being sought.

2.2. Sedimentary heterogeneity in the deposits of meandering river systems

A library of training images that incorporate the main sedimentological and stratigraphic features of meandering fluvial systems should ideally incorporate heterogeneities at different scales. Significant sedimentary heterogeneities that can be observed in fluvial successions deposited by meandering rivers occur at a range of spatial scales, and include those relating to: (i) stratigraphic architecture determined by the distribution of channel-belt and floodplain deposits; (ii) internal architecture of channel belts determined by the distribution of channel-fill and point-bar deposits; (iii) intra-bar variations in the relative proportion of sand and mud, vertically and horizontally. Such lithological heterogeneities have

long-been recognised in the deposits of meandering rivers (Jackson, 1976). From an applied perspective, such lithological heterogeneities are important because they affect fluid-flow behaviour over a range of scales (Corbett et al., 2012; Hovadik and Larue, 2007).

Some common examples of complex sedimentary architectures that give rise to the configuration and the lithological heterogeneity in the deposits of meandering fluvial systems are depicted in Fig. 2; their origins and form are summarised below.

- The migration of river channels over time results in erosion of sediments from the outer bank and sedimentation occurring via accretion on the inner bank. The gradual lateral accretion of successive units forms a point bar on the inner part of a developing meander loop. In sand-rich fluvial systems, resultant accumulated lateral-accretion architectural elements commonly form volumetrically significant sand-bodies with good reservoir potential composed internally of a coset of lateral-accretion units. Each lateral-accretion unit may be separated from its neighbouring unit within the overall point-bar element by thin lower-permeability beds. Commonly, such beds take the form of drapes on successive bar-front surfaces, which themselves accumulate during episodes of reduced flow in the aftermath of flood events (Miall, 2016).

- Some lateral-accretion units are characterized by 'inclined heterolithic stratification' (IHS), a term introduced to describe shallow-dipping heterogeneous point-bar deposits whose strata show original depositional dip (Thomas et al., 1987). Muddy IHS, in either fluvial or tidally influenced channels, may represent baffles that can hinder or impede fluid flow in otherwise sand-prone point-bar deposits (Hubbard, 2011).

- Different styles of baffling can be developed within a laterally accreting point-bar element. The distribution of intra-bar-scale heterogeneities is dependent, in part, on the growth mechanisms of the point bars and on the trajectories of the formative meanders. For example, unlike meanders undergoing simple expansion (i.e., lateral growth), translating (i.e., downstream migrating) meanders are characterized by areas where deposition takes place on concave banks, leading to the deposition of mud-prone counter-point-bar deposits (Ielpi and Ghinassi, 2014; Nanson and Page, 1983).

- High-sinuosity fluvial-channel deposits commonly display fining-upward sequences in which the coarsest-grained sediment accumulations are deposited in the lower portions of point-bar units. These results from energy dissipation associated with the helical flow in the channel (Miall, 2016). Moreover, sediments forming point-bar deposits also commonly display a trend of downstream decrease in grainsize, especially downstream of a meander-bend apex, in relation to changes in flow direction around the bend (Bluck, 1971 and Wood 1989).

These commonly occurring types of lithological heterogeneity give rise to different forms and degrees of non-stationarity, which need to be accounted for (i) in TIs that seek to depict the range of architectural

styles common in point-bar deposits associated with meandering-river succession, (ii) by means of auxiliary variable maps intended to enable effective training-image application, and (iii) in resulting MPS models (de Vries et al., 2009).
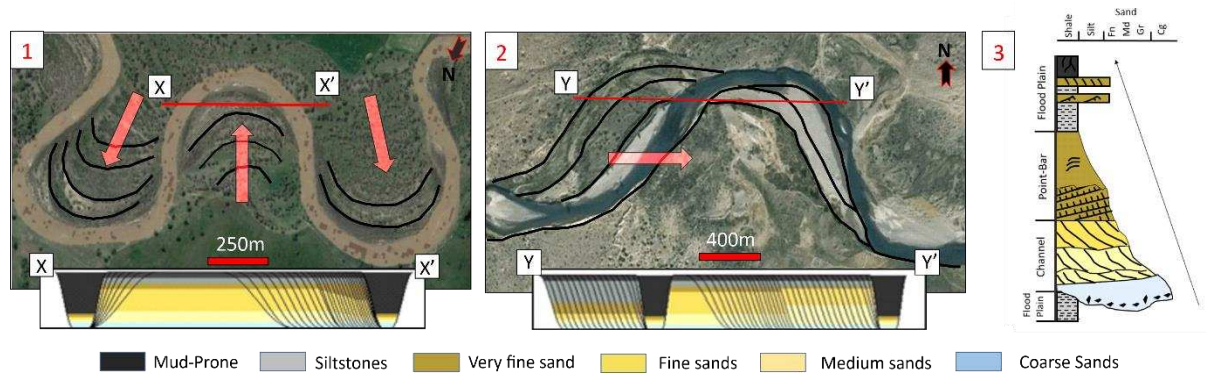
Figure 2. Two examples of point bars and their deposits associated with meanders undergoing expansion (1-Powder River, US (45°19´34.43"N-105°31´43.43"W) and translation (2-Chubut River, Argentina (42°31´26.33"S-70°32´53.24"W). Cross-sections resulting from PB-SAND forward stratigraphic model runs (X-X´ and Y-Y´) show accreted deposits with typical fining-upward trends (3). Red arrows indicate the accretion trajectory of point bars associated with the different types of meander transformations. Grainsize categories are for illustration only and may vary considerably in natural examples. These two images are shown to illustrate accretion geometries associated with meander expansion and translation, as incorporated in the training images constructed and employed in this work.

3. METHODOLOGY

A workflow has been developed for the creation of training images and their application to MPS simulations. A detailed explanation of the steps undertaken for building the TIs is provided. Six different TIs are then utilized to demonstrate their use in MPS simulations with SNESIM and DEESSE, making use of auxiliary variables to achieve the desired trends in facies distribution and orientation.

To construct TIs that include fundamental features of the facies architecture of fluvial point bars and meander belts, a workflow has been established (Fig. 3) whereby a forward stratigraphic model of meander-belt sedimentary architectures (Point-Bar Stratigraphic Architecture Numerical Deduction; PB-SAND (Yan et al., 2017, 2019, 2020) has been informed by sedimentological data drawn from a relational database (Fluvial Architecture Knowledge Transfer System; FAKTS; Colombera et al., 2012a, 2012b; 2013, 2017). The joint application of PB-SAND and FAKTS allows reproduction of the sedimentological features of interest in this particular study. Of note, TIs have been created that embody different styles of sedimentary architecture that are common in high-sinuosity fluvial environments, associated with different modes of meander transformation. Utilising this workflow, a TI library has been created that includes different TIs representing idealized stratigraphic architectures applicable to different modelling scenarios (Fig. 3).
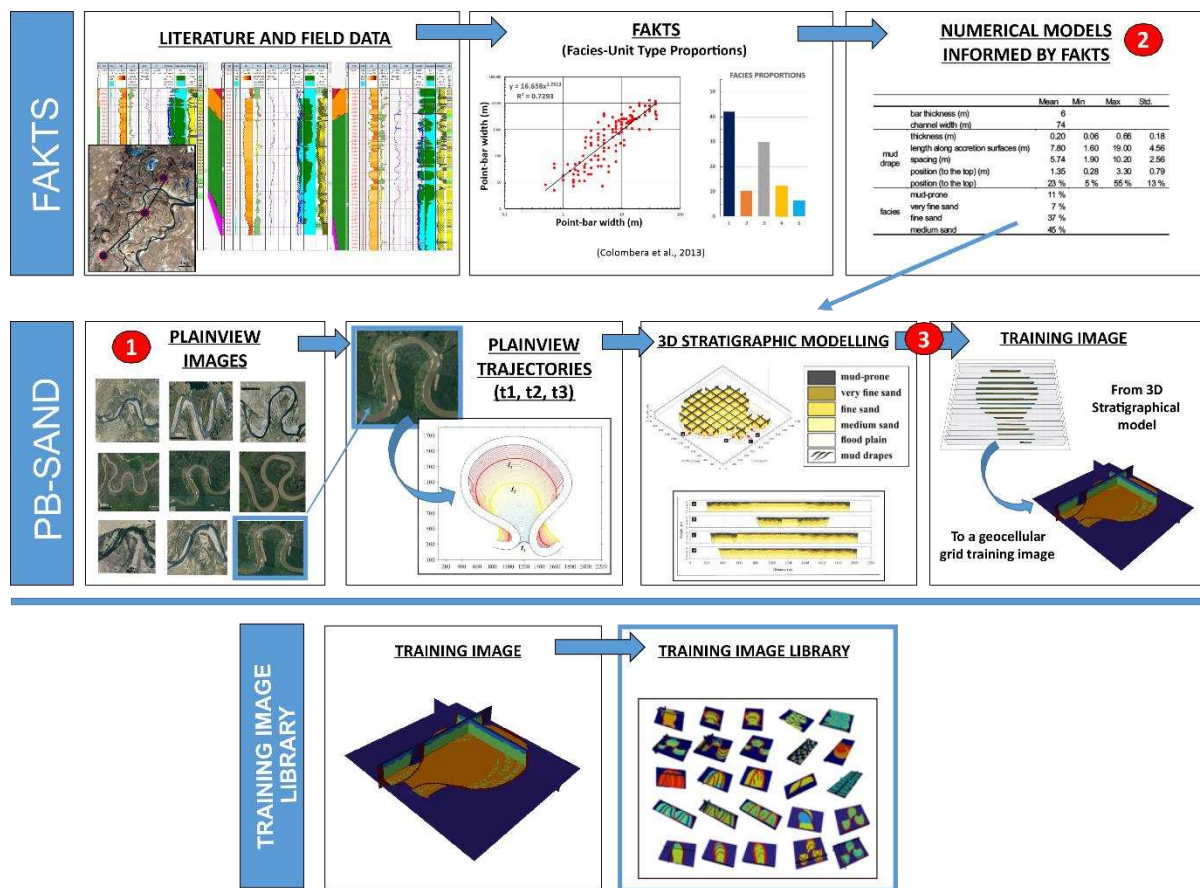
Figure 3. A training image is created following a three-step process, as follows: (1) derivation of quantitative information on facies architecture from geological analogues stored in FAKTS (e.g., facies proportions, channel geometry), to be employed as input to PB-SAND; (2) specification of trajectories tracking channel planform evolution (e.g., as captured from time-lapse satellite images), to be fed as input to PB-SAND; (3) PB-SAND simulation of meander-belt facies architectures, whereby geometries of bar accretion are modelled deterministically and facies distributions are simulated stochastically. 3D vector models produced by PB-SAND are then converted into gridded geocellular models that can be used as MPS training images. A set of training images is created using this workflow that serves as a training-image library.

3.1. PB-SAND

The Point-Bar Sedimentary Architecture Numerical Deduction (PB-SAND), coded in Matlab and C#, is a forward stratigraphic model designed to reconstruct and predict the complex spatial-temporal evolution of a variety of meandering river behaviours. The software simulates the complex spatio-temporal migratory evolution of fluvial meanders, their generated bar forms and the associated lithofacies distributions that accumulate as heterogeneous fluvial successions (Yan et al., 2017).

PB-SAND can be applied to explore and gain improved understanding of relationships between evolutionary channel trajectories and preserved lithofacies distributions, allowing reproduction of the stratigraphic heterogeneity of fluvial meandering systems at different temporal and spatial scales and in three spatial dimensions.

Based on time-lapse plan-view trajectories of channel courses (e.g., as captured from satellite images; cf. Figure 2) PB-SAND can reconstruct the channel-belt sedimentary architectures that arise from the complex spatio-temporal evolution of meandering rivers; facies characteristics in the modelled architectures will reflect the type of meander-bend transformation, the channel sinuosity, the stream-wise distance away from meander apices, and the position of inflection points of a meander loop (Yan et al., 2019). In addition to the centrelines that track the course of a river channel at different times, PB-SAND requires definition of several other parameters, which vary depending on the type of meander-bend transformation, and which include the river-channel hydraulic geometry (maximum bankfull depth, width) and descriptions of the types and arrangement of lithologies forming point-bar and channel-fill deposits (Yan et al., 2021). Inputs to constrain channel-form and bar geometries can be acquired from different sources such as well data (electrical logs, core data, etc), field-based measurements from outcrops and modern systems, satellite images, or – as done in this study – from a relational database (FAKTS) that stores the required inputs.

3.2. FAKTS

The Fluvial Architecture Knowledge Transfer System (FAKTS) is a MySQL relational database that stores quantified sedimentological data from modern systems and analogue ancient fluvial successions (Colombera et al., 2012a, b; 2013, 2017). FAKTS satisfies the long-recognized need for inclusion of quantitative inputs in facies models, which improves the value of facies models as a reference for comparison, interpretation and subsurface prediction.

FAKTS uses end-member styles of fluvial geomorphology to classify facies models by type of facies, facies associations and facies relationships that tend to occur in a particular environment. FAKTS allows determination of appropriate geological analogues to subsurface reservoir successions (Colombera et al., 2012a). This is the case that applies for this particular research where FAKTS provides the required inputs to PB-SAND.

3.3. Construction of training images

The TIs constructed in this work are scale-independent, hence only a relative scaling between channel-fill and barform deposits is specified, on the basis of analogue data from FAKTS (Colombera et al., 2012a, b; 2013, 2017, 2018). In PB-SAND outputs, the stratigraphic complexity of point-bar deposits is characterized by bar-accretion geometries and the presence of genetically related channel fills, sitting in a background of fine-grained overbank deposits. By default, a representative fining-upward point-bar succession is modelled, though the facies trends can be customized. PB-SAND incorporates a number of facies types specified by users, and which relate to different grainsize categories (e.g., gravel, clay). Additional lithofacies types include the following: (i) mud that is deposited on accretion surfaces to form drapes during stages of low energy or slack water; (ii) mud that accumulates in undisturbed floodplain areas between point-bar elements; and (iii) conglomerates or breccias that accumulate on the

channel thalweg floor as a result of localized reworking of channel banks (e.g., intraformational mud-clast breccias) (Miall, 1996).

In this study, training images that incorporate three, four or five facies were created for the purpose of testing different geomodelling scenarios. PB-SAND outputs are vector-based, grid-free graphics. This output is converted to a 3D geocellular grid, which can be outputted as an ASCII format text file or GSLib file for importing into industry-standard software applications. The resulting TIs are idealized and scale independent. Examples of the produced training images can be seen in Figure 4.

Although MPS modelling codes are known to work best with stationary training images, all the 3D training images created for the purpose of this research represent inherently non-stationary fluvial architectures. This means that some of the lithological trends (e.g., point-bar fining-upward) are incorporated in the training image itself. However, the reproduction of other forms of non-stationarity (e.g., spatial variations in proportions of deposits) is only attempted through the application of auxiliary variables when performing MPS simulations (see below).

3.4. Training-image selection

From PB-SAND outputs, two geometric frameworks were selected that are representative of meander-belt architectures associated with meander translation and expansion, respectively (Fig.4). For each of these two architectural frameworks, a set of three alternative TIs were created using a different number of facies. The aim of this is to simulate different categories of lithology and different types of facies trends, each of which serves a different geomodelling purpose.

1) Three-facies training image. In this case, the training image only incorporates lithological categories representing point-bar (sand-prone), floodplain (mud-prone) and channel-fill (mud-prone) deposits. A TI of this type is applicable in contexts of prospect evaluation, or where intra-point-bar sedimentary heterogeneity is considered negligible or not important.

2) Four-facies training image. In addition to the previously mentioned facies, training images of this type also include a separate category for muds that are deposited as drapes on the bar fronts and that are thus oriented along lateral-accretion surfaces. Therefore, these training images include: point-bar (sand-prone), floodplain, channel-fill and bar-front-mud (all mud-prone) facies. A TI of this type is applicable in contexts requiring assessment of intra-point-bar compartmentalization.

3) Five-facies training image. Three additional types of sandy facies within point-bar (meander expansion and translation) and counterpoint-bar (meander translation) deposits are defined in terms of grainsize (coarse, medium and fine sands) to portray fining-upward (meander expansion and translation) and downstream-fining (meander translation) trends. A TI of this type is applicable in situations where prediction of intra-point-bar petrophysical heterogeneity is deemed important.

The size of the geobodies that are to be modelled in the simulation grid is determined by the number of cells and the cell size of the training image, in accordance with the number of cells and cell size of the simulation grid. Vector-based output from PB-SAND can be rasterized at any resolution. The larger the size and/or resolution (number of cells) of the TI, the longer it will take to complete a realization using it. Since an objective of this study is to develop a workflow that delivers a realization in less than 10 minutes – a runtime considered to be standard in industry – using a standard desktop computer (of 2019 vintage), upscaling of the training images is required. Training-image grid upscaling may result in significant loss of sedimentological detail, but the TIs included in the library are all scale-independent, allowing users to set a resolution that preserves the desired features.

3.5. MPS algorithms: SNESIM and DEESSE

The training images have been applied in workflows for the simulation of meandering fluvial systems using the modelling algorithms SNESIM (Strebelle, 2002) and DEESSE (Mariethoz et al., 2010). A calibration process based on trial and error has been employed to determine appropriate inputs for parameters that control TI scan and grid simulation, for both SNESIM and DEESSE. This has been achieved by trialling different values for input parameters, with consideration of runtime performance. Some of these parameters are similar or equivalent for SNESIM and DEESSE (e.g., search mask/neighbourhood) others are unique and only apply to a particular code (e.g., number of replicates in SNESIM, distance threshold "t" in DEESSE).

The numbers of facies in the training images have a significant impact on the computational time of both SNESIM (Strebelle, 2002) and DEESSE (Mariethoz et al., 2010). Input parameters have been adjusted to a runtime target of 10 minutes or less. The same facies proportions for the different facies included in the training images have been specified as the target proportions for realizations of both SNESIM and DEESSE. In SNESIM, the modelled facies proportions are allowed to vary from the input facies proportions if the servosystem value 'λ' is different from 0, or if a trend is included using an auxiliary variable. For this study, the servosystem value was set to 0.5, and probability grids were employed, so a discrepancy between target and output proportions is expected.

The number of nodes considered during scan and simulation depends on the size and shape of the search mask or neighbourhood, i.e., of geometric templates defined as a set of cells with elliptical, circular or rectangular shape, and specified in terms of radius, azimuth, strike and rake. The larger the search mask, the longer the time per realization (Meerschman et al., 2013). In DEESSE, the radius of the search neighbourhood can vary according to the number of nodes that are being simulated. (i.e., the size of the radius will progressively decrease when the number of simulated nodes increases). A number of strategies have been introduced for optimizing search-mask or search neighbourhood definition. Riou et al. (2015), in application to channelized architectures, proposed the application of a search radius of

1.5 times the width of the largest channel units, and recommended isotropic search neighbourhoods as the most robust option for capturing some of the patterns expected in fluvial meandering systems.

In SNESIM, so-called 'multigrids' and 'subgrids' are used to configure the search mask so as to store the conditional probabilities efficiently. The purpose is to capture large-scale structures using a relative small search mask with a relatively small number of nodes. The larger the multigrid size the fewer the nodes that need to be considered in a particular grid. In this study, four multigrids have been used to run the simulations, as preliminary work indicated that this setting results in reasonably short runtime; the four multigrids have each been divided into four subgrids, which allow locating a larger number of conditioning data during simulation. The runtime increases with increasing minimum number of replicates (Strebelle, 2002); a minimum number of replications between 5 and 10 has been chosen.

In the TI-scan process performed by DEESSE, a distance threshold 't' is used to define the tolerance within which a pattern is recognized to match; the maximum fraction of TI to scan ('f') can also be specified (Mariethoz et al., 2010). Runtime increases with decreasing values of 't' and increasing values of 'f' (Meerschman et al., 2013). In DEESSE, the combination of number of nodes (n), distance threshold (t), and maximum scanned fraction (f) will have a significant impact on computation time. Therefore, changes to these parameters will need to be considered jointly. According to Meerschman et al. (2013) important considerations can be made as follows: (i) pattern-reproduction performance improves when 'n' is larger, 't' is closer to 0, and 'f' is closer to 1, but at the expense of realization runtime; (ii) variations in 't' and 'n' influence significantly the degree to which the patterns from the training image are reproduced in the simulation grid. However, 'f' has a much smaller effect on the simulation quality; (iii) reducing the scanned fraction 'f' of the TI allows substantial computational gains without degrading pattern reproduction as long as the TI contains a large enough number of reproducible patterns; (iv) a small 'f' value for TIs may lead to TI under-sampling and thus affect simulation results, but usually results in large computation gains without substantial decrease in simulations quality. The choice of input parameters to DEESSE was guided by these considerations. Table 1 includes all the parameters used for every simulation presented in this study.

3.6. Auxiliary variables (trends)

To employ the TIs for modelling the stratal architecture of a particular fluvial meandering system, a hierarchical approach to facies modelling has been taken. This is in part achieved through the use of auxiliary variables as means to force the incorporation of expected or desired geological features within the models.

For obtaining representative statistics, MPS algorithms commonly require stationary TIs. However, sedimentary bodies and associated facies characteristics and distributions tend to vary in space, i.e., are non-stationary. To be able to incorporate – at least in part – non-stationary features in the simulations, auxiliary variable grids (Chugunova at al., 2008) have been employed. Auxiliary variables are gridded

properties that describe a spatial trend in the property being modelled. They also facilitate the reproduction of nested architectures, whereby simulations are undertaken at multiple scales, to enable reproduction of heterogeneities.

Table 1 The parameters employed in the simulations whose outputs are discussed. SM: Search Mask, SN: Search Neighbourhood N: Nodes, Serv: Servosystem, Rep: Number of replicates, MG: Multigrids, SG: Subgrid, Tau: Tau Model weight values, SN: Search Neighbourhood, DT: Distance Threshold, F: maximum fraction of TI to scan, SR: Support Radius and DTR: Deactivation Threshold Radius.

		SNESIM input parameters						DEESSE input parameters					
		SM	N	Serv	Rep	MG	SG	Tau	SN	N	DT	F	SR	DTR
Meander expansion TIs	**Case 1**	2000x 2000y 10z	60	0.5	10	4	4	2, 1	20x 20y 8z	30	0.15	0.3	7	5
	Case 2	2000x 2000y 10z	60	0.5	10	4	4	2, 1	20x 20y 8z	30	0.2	0.3	10	8
	Case 3	4000x 3000y 4z	60	0.5	10	4	4	2, 1	20x 20y 4z	30	0.2	0.3	10	6
Meander translation TIs	**Case 4**	5000x 5000y 10z	60	0.5	5	4	4	2, 1	20x 20y 5z	30	0.2	0.5	12	10
	Case 5	5000x 5000y 10z	60	0.5	5	4	4	2, 1	18x 18y 4z	35	0.15	0.5	10	7
	Case 6	5000x 5000y 5z	60	0.5	5	4	4	2, 1	15x 15y 5z	40	0.15	0.5	10	8

Auxiliary variables in the form of 2D or 3D grids are routinely used for forcing the reproduction of spatial variations in modelled properties at different levels (e.g., in mean body thickness, grainsize). These auxiliary variables allow resultant models to account for non-stationarity relating to scaling effects (scaling maps that describe variations in space of the scale of certain features), variations in orientations of architectural elements (rotation maps), variations in the facies proportions (probability maps), and differentiation of regions characterized by different types of lithological heterogeneities (region maps). Probability maps are used as part of the proposed workflow to facilitate the reproduction of geological features associated with the channel belts of meandering rivers.

In the proposed workflow, probability maps have also been used to ensure realistic spatial transitions between facies, particularly between channel-belt and floodplain facies, and the reproduction in the simulations of specific sedimentological features, such as planform cut-bank geometries, and variations in facies proportions. Auxiliary variables also facilitate the incorporation of relationships between small-scale and large-scale features in a reservoir model (see below).

Auxiliary variable grids have been used in the developed workflow, consisting of grids that specify the probability of modelling categories. The object-based modelling tool of Schlumberger Petrel® was used to create probability regions. These regions represent: (i) the axial part of a sand fairway that could

represent an amalgamated channel belt or valley fill (90% probability of channel deposits); (ii) an area that can only be occupied by floodplain deposits (100% probability of occurrence of mud-prone overbank sediments); and (iii) a buffer area that is defined with the scope to reproduce realistic channel-to-overbank transitions, whereby the channel belts would have some rugosity in planform and mud plugs would border the outer side of the belts (see Fig. 4). The same probability grids have been applied to all simulations, but a total of 3 different grids for each of the 3 TI types (3, 4 and 5 facies) have been created, which will differ with respect to probability values assigned to each region (cf. tables in Fig. 4).

3-FACIES MODELS

		Floodplain	Channel-Fill	Point-Bar
ZONE 1		0.1	0.55	0.35
ZONE 2		0.5	0.250	0.250
ZONE 3		1	0	0

4-FACIES MODELS

		Floodplain	Channel-Fill	Bar-Front Mud	Point-Bar
ZONE 1		0.1	0.3	0.3	0.3
ZONE 2		0.5	0.167	0.167	0.167
ZONE 3		1	0	0	0

5-FACIES MODELS

		Floodplain	Channel-Fill	Fine Sands	Medium Sands	Coarse Sands
ZONE 1		0.1	0.225	0.225	0.225	0.225
ZONE 2		0.5	0.125	0.125	0.125	0.125
ZONE 3		1	0	0	0	0
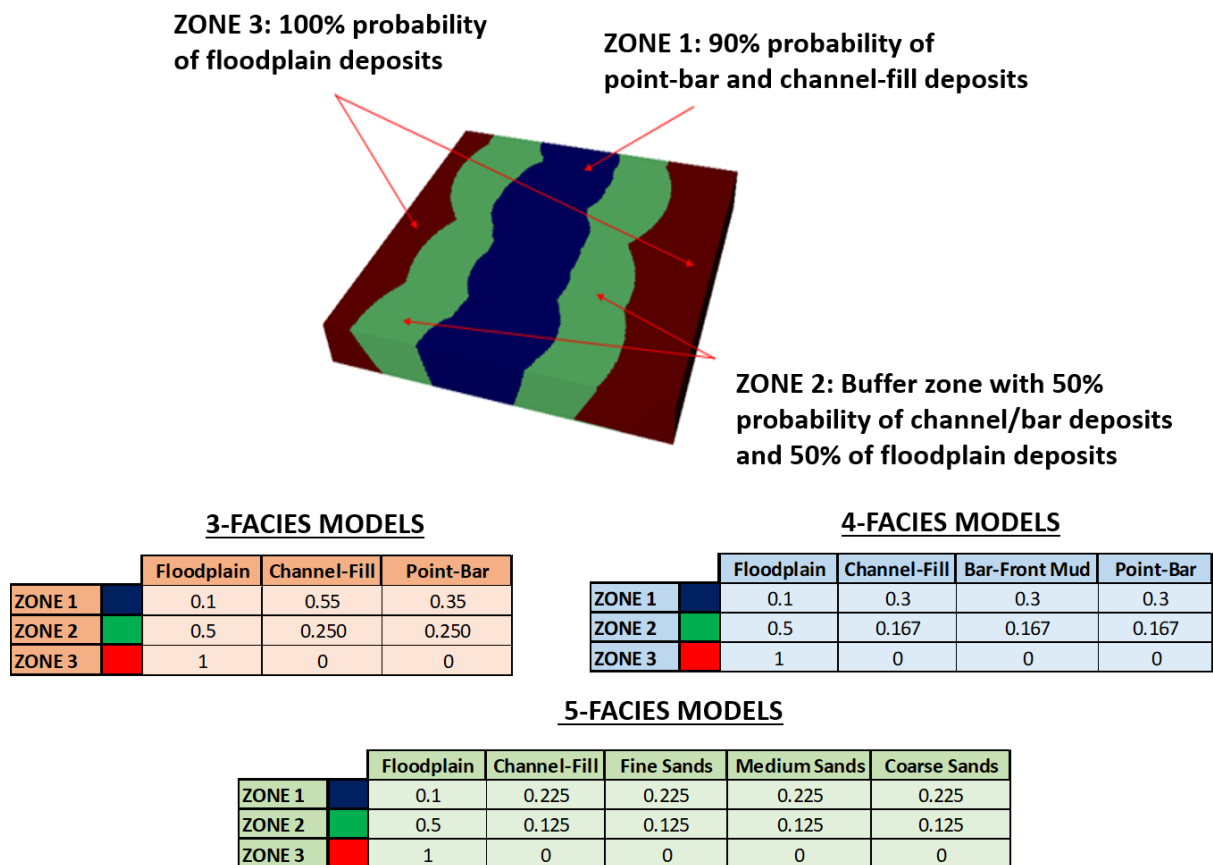
Figure 4. Example of a probability grid that may be applied to reproduce facies distributions in a channel-belt or valley-fill unit. In the grid, 3 different zones are created, within which the probability of occurrence of the facies varies. The tables represent the 3 different probability scenarios that will be used in the application of training images that include 3, 4 and 5 facies (see main text and Table 1).

The functioning of probability grids differs between SNESIM and DEESSE. In SNESIM, auxiliary variables are applied based on TAU models (Journel, 2002). The probability of A jointly conditioned on B and C becomes a function of the marginal probability of A and of the two probabilities of A separately conditioned on B and C. This function depends on a parameter τ that measures the degree of redundancy between events B and C with respect to event A (Krishnan et al., 2005). Parameters that act as weights, named Tau2 and Tau1, can be controlled so that the higher Tau2 relative to Tau1 the higher is the influence of soft-probability data in controlling simulation results.

In DEESSE two main parameters control simulation outputs: the support radius (SR) and the deactivation threshold radius (DTR). The simulation process will randomly pick a data event "X" (i.e., a pattern formed by a certain number of cells) in the simulation grid, and will then try to find a similar data event considering (i) the patterns in the training images, (ii) the previously populated categories in the simulation grid, and (iii) the probabilities stored in the probability map. SR is used to identify patterns in the nodes that have been previously populated. If within the SR distance there are more informed nodes than the number of nodes, the nodes closest to "X" are those that will be populated in the realizations.

At the beginning of the simulation, prior to any cells being populated in the simulation grid, the algorithm populates facies that are recognised directly from the training image conditioned on the probabilities in the probability grid. At this stage the SR is equal or smaller than the actual search radius (RA). However, towards the end of the simulation, when most of the simulation grid is populated with informed nodes, if the RA is smaller than the DTR distance, the probability constraint mechanism is stopped. The selection of appropriate SR and DTR is a critical step when dealing with auxiliary variables in DEESSE, as it significantly affects the quality and the computation time per realization.

3.7. Model configuration and input tuning

Training images have been used that incorporate the two channel-belt geometries shown in Fig. 5, which are representative of channel-belt reaches composed of three meander bends and associated point-bar and channel-fill deposits, placed in a background of fine-grained floodplain sediment. The two architectural frameworks represent simple meander belts that are respectively undergoing meander expansion and translation. For each of these two frameworks, three different sets of modelling categories (hereafter termed 'facies', for sake of simplicity) have been considered (Table 1). Each of these sets involves different number and types of facies. The three cases are as follows: (i) 3-facies case (point-bar, channel-fill and floodplain deposits); (ii) 4-facies case (point-bar deposits, channel-fill deposits, continuous bar-front muds and floodplain deposits); and (iii) 5-facies case (coarse point-bar sands, medium point-bar sands, fine point–bar sands, channel fill and floodplain deposits). These facies configurations have been selected to run unconditional simulations, such as those that would be run for modelling undrilled prospects, since unconditional realizations are ideal for assessing the degree to which TI patterns are reproduced (Rojas et al., 2012; Manchuk et al., 2011; Manchuk and Deutsch, 2012).
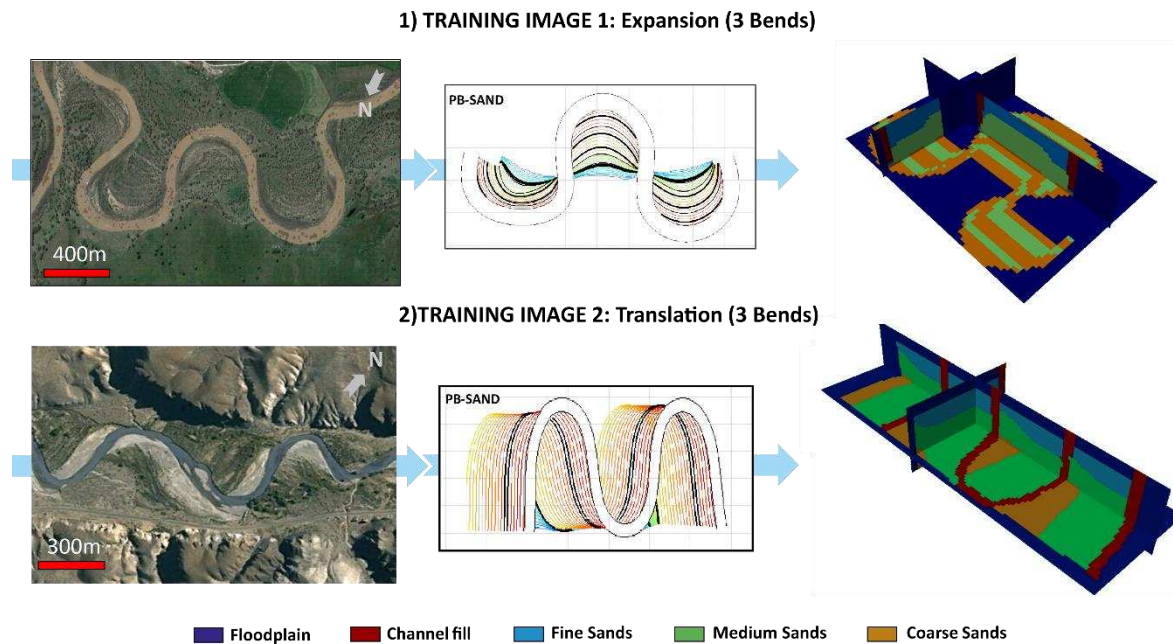
Figure 5. Two training images selected from the training-image library, which incorporate channel belts associated with two different scenarios of meander transformation: 1) meander expansion (mean sinuosity 1.55) and 2) meander translation (mean sinuosity 3.03). PB-SAND outputs of reconstructed planform evolution are also shown in the middle, showing the plan-view expression of accretion surfaces resulting from channel migration through time. The legend at the bottom applies to the gridded TIs shown on the right-hand side. Satellite imagery of meanders undergoing expansion and translation are shown for comparison.

Unconditional simulations were performed to establish preferred modelling recipes that can be paired to each training image and to each MPS modelling algorithm. SNESIM and DEESSE were run on a simulation grid with the following dimensions: 250 cells along X, 250 cells along Y and 50 cells along Z. The cell size for the simulation grid was set to X:Y:Z ratios of 20:20:0.25.

The parameters selected for every simulation in SNESIM and DEESSE, based on trial and error and aiming for a runtime below 10 minutes, are shown in Table 1.

Results are analysed and discussed according to qualitative criteria that allow evaluation of aspects of sedimentary architecture whose reproduction in the simulations is desirable. These are: (i) planform sinuosity and continuity of deposits with curvilinear geometries such as channel fills and bar-front muds; (ii) cross-sectional channelized geometry and adjacency to point-bar facies for channel-fill deposits, which act to compartmentalize point-bar sands; (iii) vertical fining-upward trends in point-bar deposits, in cases where different grainsize categories of point-bar sediments are considered; (iv) planform concavity of abandoned channel-fills being oriented towards the belt axis when placed at the transition to the overbank domain; and (v) outward fining in point-bar elements associated with expansional meanders. Additionally, for training images embodying the products of meander translation, the presence of counter-point-bar deposits (which are typically finer grained than corresponding point-bar deposits) associated with concave-bank accretion is also evaluated.

4. RESULTS

Here, an evaluation of the modelling outputs that would be generated upon application of training images created using the proposed workflow is presented. Results are shown below for the six cases that result from applying (i) the two sets of training images reflecting contrasting channel-belt accretion geometries and (ii), for each set, three facies configurations, as explained above (Section 3.4; Fig. 4). The training images were retrieved from the training-image library constructed following the workflow explained above (Sections 3.1-3.3; Figure 3). The application of training images in MPS simulations was tested using SNESIM and DEESSE, constrained through the parameters and auxiliary variable described above (Sections 3.5-3.7). Outputs of SNESIM and DEESSE are compared in terms of degree of pattern reproduction and CPU performance.

Twenty realizations were generated for each of the six simulation cases. In the figures (Figures 6-11), only one of these realizations is presented for each of the six cases. The results of the qualitative assessment of modelling outputs are also indicated in Figures 6 to 11.

4.1. Case 1: meander expansion (3 facies)

Upon application of this TI, in both SNESIM and DEESSE realizations (Fig. 6) sinuous channel-fill deposits appear relatively continuous, locally display loop geometries, and compartmentalize the sand-fairway zone where point-bar deposits are located. Stratigraphic compartmentalization created by sinuous channel-fill deposits is also evident in vertical sections of realizations delivered by SNESIM. DEESSE realizations appear slightly different in vertical sections, in which more vertically elongated features are present. Overall, both SNESIM and DEESSE successfully reproduce meandering loops typical of mud-filled plugs representing abandoned channel-fill segments over a sand fairway (fluvial channel belt).

4.2. Case 2: meander expansion (4 facies)

Case 2 was simulated using a larger training image (number of cells: 165 along x, 175 along y, 60 along z) to test the effects of image resolution in populating geobodies with better defined geometries in the selected simulation grid (Fig. 7). SNESIM simulations delivered results in less than 7 minutes, on average. However, for simulations performed according to the devised workflow using DEESSE, in order to complete simulations within the 10-minute runtime target, the TI had to be set to a lower resolution (76x80x30). Although DEESSE realizations contain geobodies that are significantly smaller than those generated by SNESIM due to the different size of the TI, realizations are relatively similar in terms of geological patterns they incorporate. Curvilinear shapes are evident in plan-view sections, corresponding to channel-fill deposits and mud-front facies. Channel-fill deposits create compartments separating volumes of point-bar facies, but lack the expected continuity in both SNESIM and DEESSE realizations. Plan-view sections show bar-front muds that are sinuous and delineate a second type of

compartments within the point-bar facies, separating different sand-prone packages. Compartmentalization by thick mud-prone packages that drape accretion surfaces are also evident in most of the realizations. In vertical sections, channel-fill deposits exhibit a channelized shape. However, both channel-fill and bar-front-mud bodies are excessively elongated vertically in DEESSE simulations, similarly to Case 1.
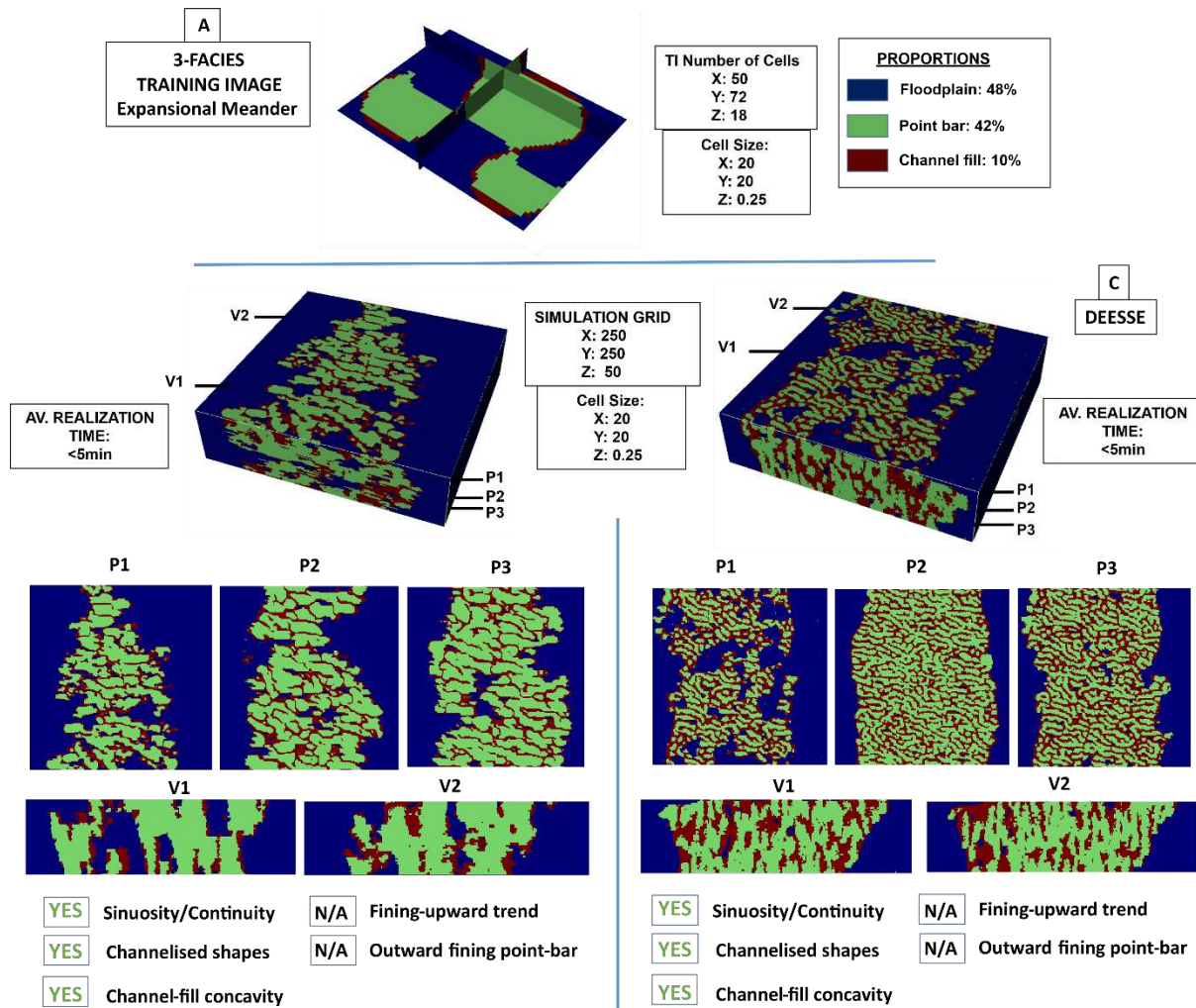
Figure 6. Representative simulation results for the 3-facies training image for meander belts with expansional meanders (case 1). (A) Employed training image. Number of cells, cell size and proportions are indicated. Simulations performed for SNESIM (B) and DEESSE (C) are presented as block models in perspective view, together with 3 plan-view sections (P1, P2 and P3) and 2 vertical sections (V1 and V2) for each. A summary of the number of cells for the simulation grid is reported between part B and C. Below the vertical sections, a qualitative assessment of the realizations is presented for each simulation method.

4.3. Case 3: meander expansion (5 facies)

These simulations attempted to model different types of sandy point-bar facies including the characteristic fining-upward trend common in expansional point-bar elements (Fig. 8).

In horizontal sections, realizations created by both SNESIM and DEESSE demonstrate the simulated lateral juxtaposition of different point-bar elements deposited through the sand-fairway region. Channel-fill deposits are seen as remnant channel-fill plugs that have limited continuity and sinuosity; these only locally compartmentalize point-bar sands, as is common in many documented successions.

Vertically, a fining-upward trend has been successfully reproduced by both SNESIM and DEESSE, with channel-deposits located at the margins of point-bar units. Model outputs are characterized by vertically stacked bar-and-channel deposits locally separated by remnants of overbank deposits, such that point-bar tops are mostly preserved.

In general terms, realizations performed using both SNESIM and DEESSE show aspects of geological realism; it is possible to differentiate different types of sand-prone units located in isolated compartments. No major differences in runtime were observed between SNESIM and DEESSE.
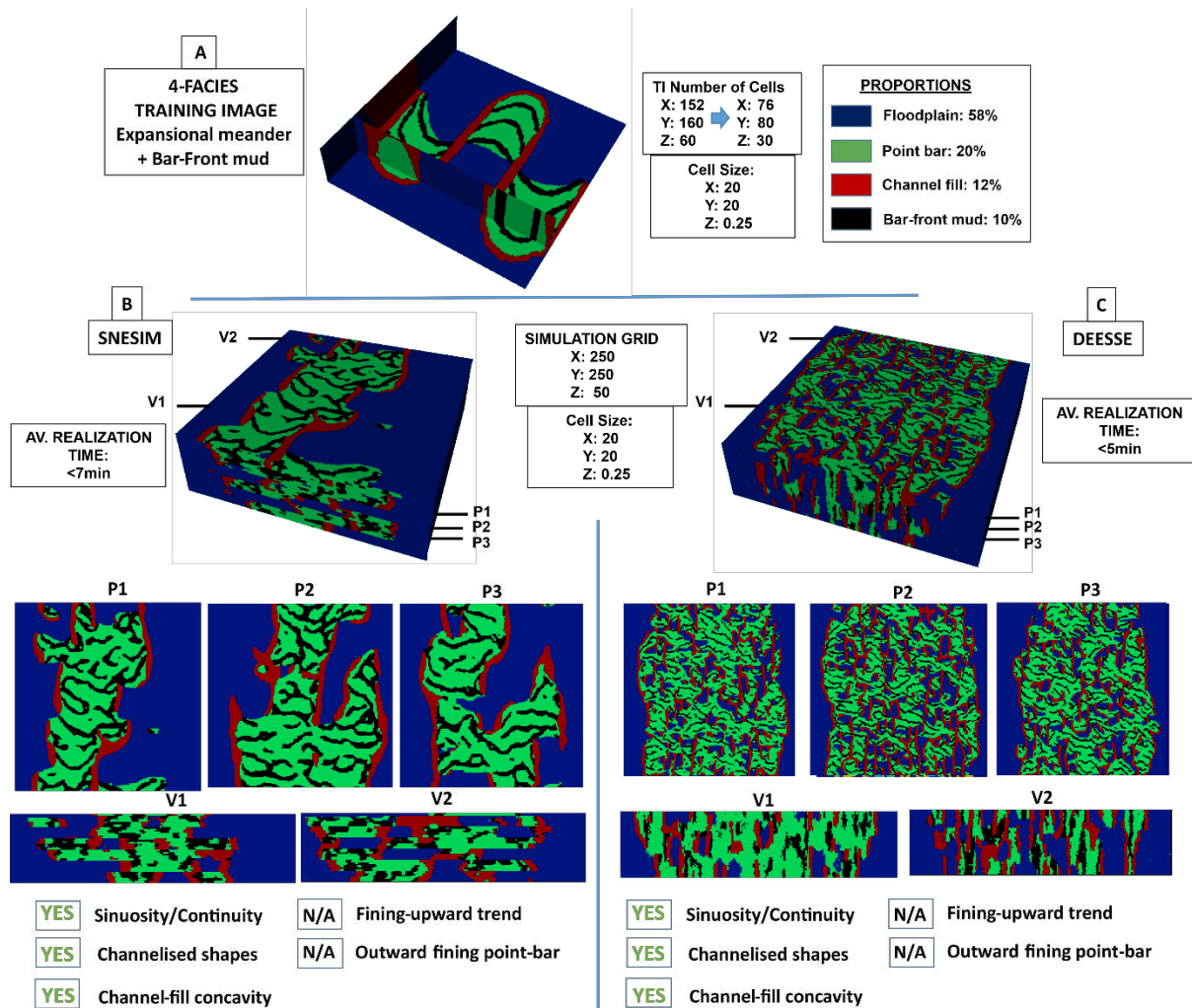
Figure 7: Representative simulation results for the 4-facies training image for meander belts with expansional meanders (case 2). (A) Employed training image. Number of cells, cell size and proportions are indicated. Simulations performed for SNESIM (B) and DEESSE (C) are presented as block models in perspective view, together with 3 plan-view sections (P1, P2 and P3) and 2 vertical sections (V1 and V2) for each. A summary of the number of cells for the simulation grid is reported between part B and C. Below the vertical sections, a qualitative assessment of the realizations is presented for each simulation method.
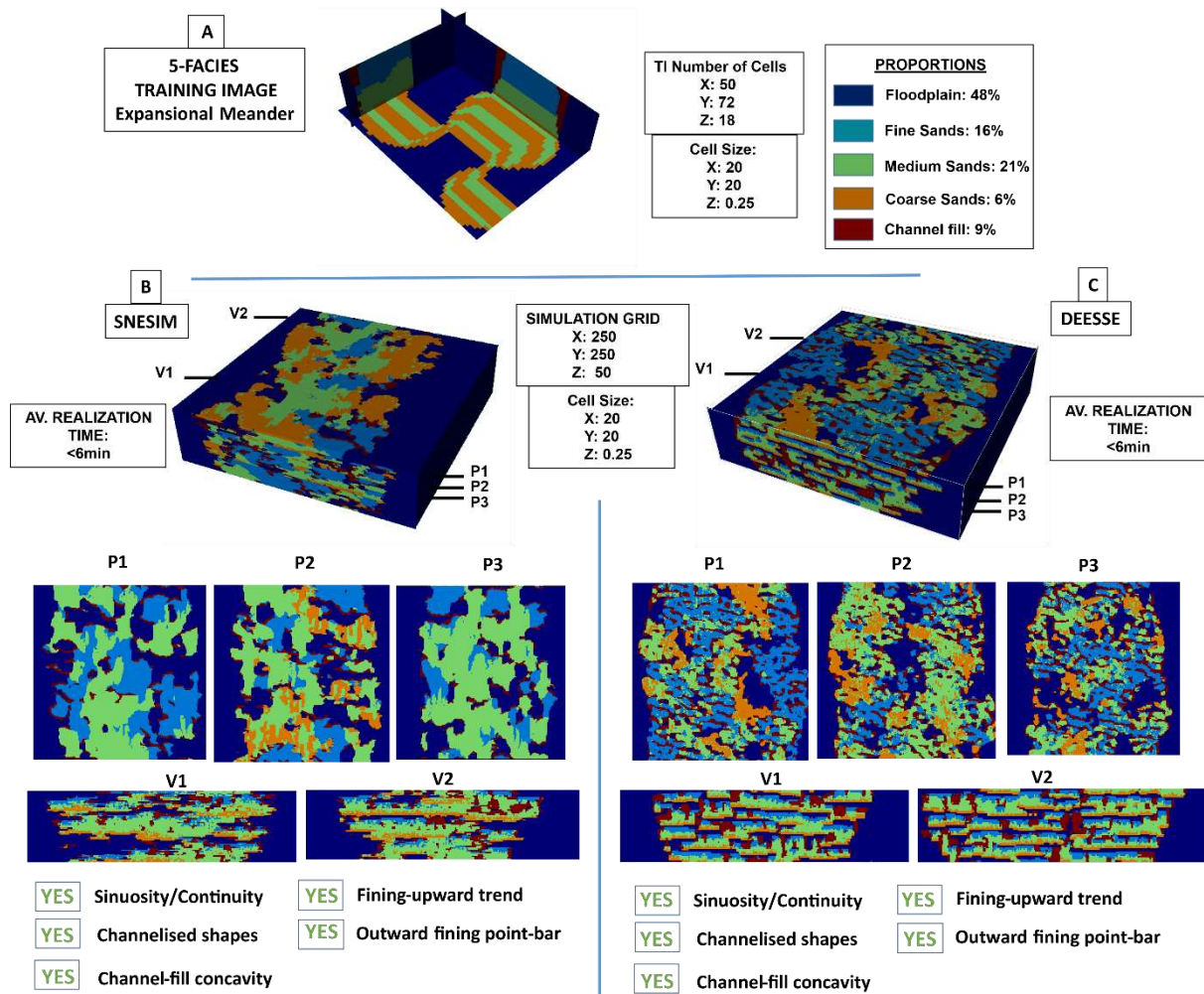
Figure 8: Representative simulation results for the 5-facies training image for meander belts with expansional meanders (case 3). (A) Employed training image. Number of cells, cell size and proportions are indicated. Simulations performed for SNESIM (B) and DEESSE (C) are presented as block models in perspective view, together with 3 plan-view sections (P1, P2 and P3) and 2 vertical sections (V1 and V2) for each. A summary of the number of cells for the simulation grid is reported between part B and C. Below the vertical sections, a qualitative assessment of the realizations is presented for each simulation method.

4.4. Case 4: meander translation (3 facies)

On horizontal planes, simulations performed using both SNESIM and DEESSE demonstrate channel-fill geobodies that appear as low-sinuosity linear features that are oriented perpendicular to the direction of the sand-fairway axis (Fig. 9) and that are laterally discontinuous. Compartments are locally created by the channel-fill deposits, which do not however exhibit loop geometries. In vertical sections, channelized features are recognizable as channel deposits in simulations delivered by SNESIM. However, DEESSE realizations include oversized channel-fill geobodies. Overall, geometries of geobodies produced by SNESIM and DEESSE differ from the ones in the original training image. Notably, channel-fill deposits appear overly elongated along a direction that is perpendicular to the sand-fairway axis.

20
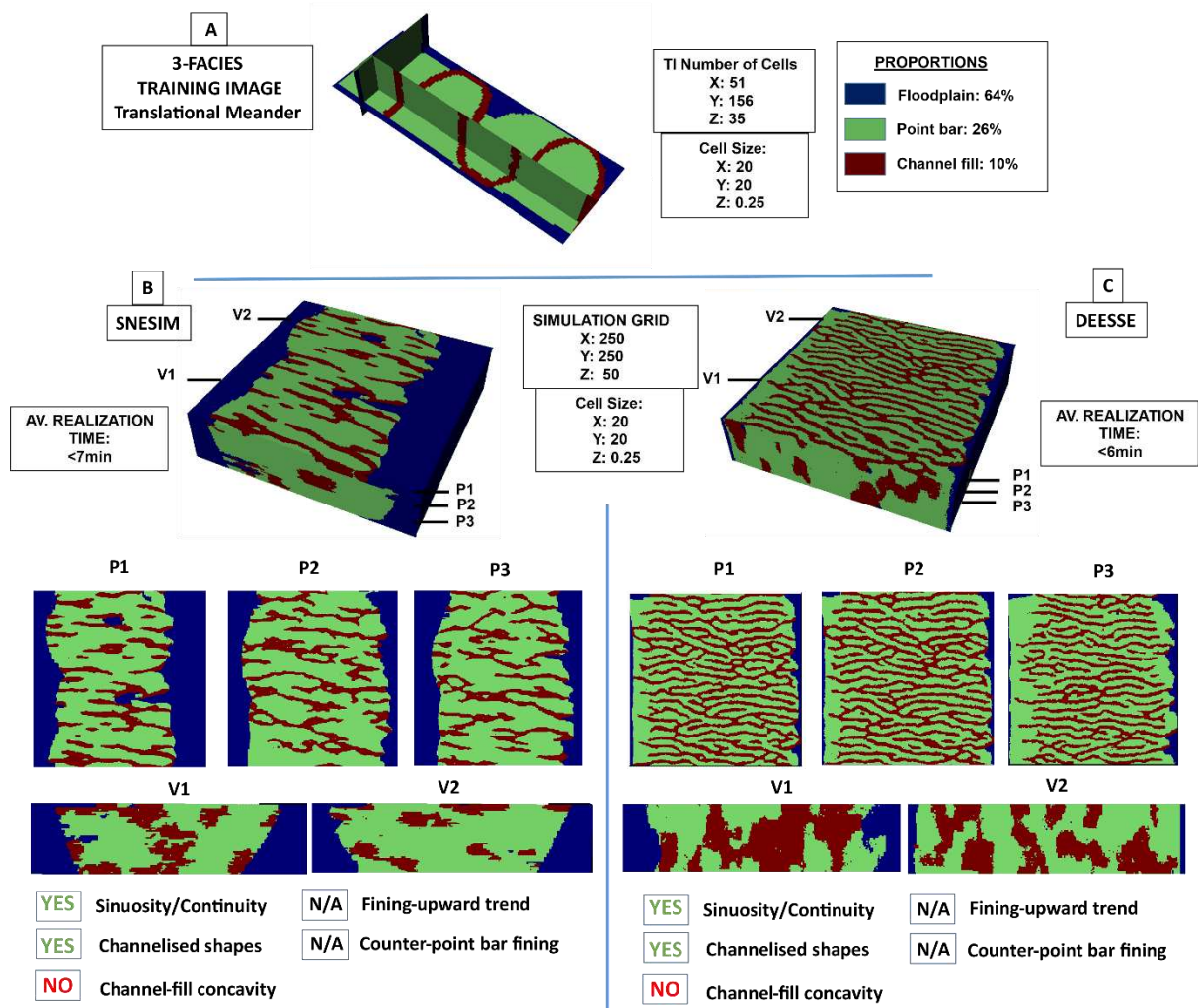
Figure 9: Representative simulation results for the 3-facies training image for meander belts with downstream translating meanders (case 4). (A) Employed training image. Number of cells, cell size and proportions are indicated. Simulations performed for SNESIM (B) and DEESSE (C) are presented as block models in perspective view, together with 3 plan-view sections (P1, P2 and P3) and 2 vertical sections (V1 and V2) for each. A summary of the number of cells for the simulation grid is reported between part B and C. Below the vertical sections, a qualitative assessment of the realizations is presented for each simulation method.

4.5. Case 5: meander translation (4 facies)

Similar to Case 4, considerable time was required to satisfactorily tune input parameters to DEESSE. Both SNESIM and DEESSE realizations produced using this TI (Fig. 10) include channel-fill geobodies and mud-prone packages that appear as low-sinuosity ribbons elongated perpendicularly to the sand-fairway axis, similarly to Case 4. Both mud-prone packages and channel-fill deposits interrupt the continuity of sandy point-bar deposits. However, similarly to the 3-facies scenario, channel-fill meander-loop elements are rarely reproduced, since channel fills appear as continuous features perpendicular to the channel-belt axis. Furthermore, delivered realizations included sharp transitions between floodplain and channel-belt facies, and in most of the cases simulations incorporated less than 50% of floodplain facies, as embodied in the probability grid selected for this simulation (Fig. 4). In

21

vertical sections, channel-fill deposits rendered by DEESSE have more unrealistic shapes and aspect ratios that those generated by SNESIM.
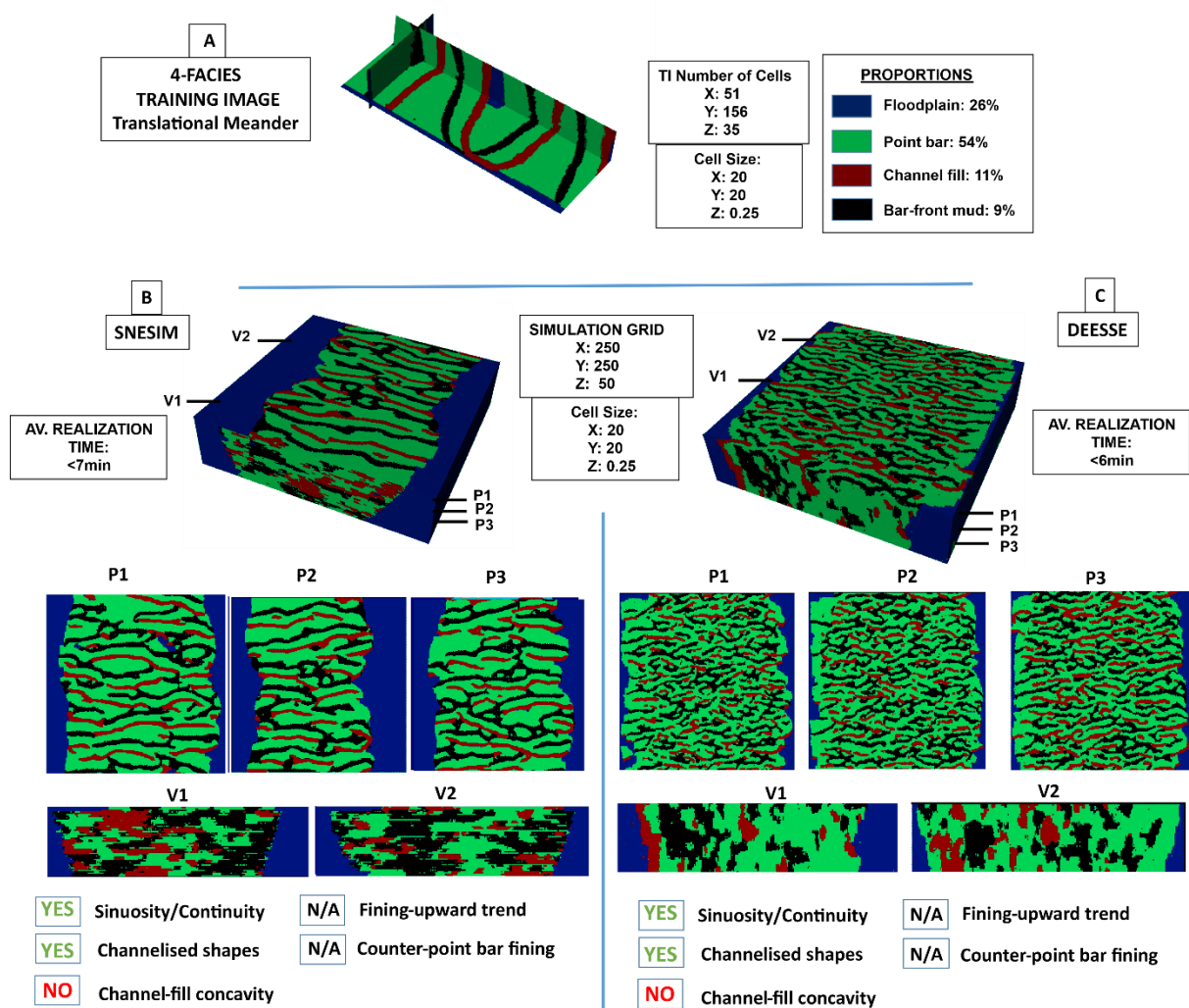
Figure 10: Representative simulation results for the 4-facies training image for meander belts with downstream translating meanders (case 5). (A) Employed training image. Number of cells, cell size and proportions are indicated. Simulations performed for SNESIM (B) and DEESSE (C) are presented as block models in perspective view, together with 3 plan-view sections (P1, P2 and P3) and 2 vertical sections (V1 and V2) for each. A summary of the number of cells for the simulation grid is reported between part B and C. Below the vertical sections, a qualitative assessment of the realizations is presented for each simulation method.

4.6. Case 6: meander translation (5 facies)

These realizations include different types of bar deposits (grainsize categories) located within the channel belt (Fig. 11). Compartmentalization determined by muddy abandoned channel-fill deposits is oriented dominantly perpendicular to the channel-belt axis. However, similarly to cases 4 and 5, the continuity of abandoned channel-fill elements is limited. Sinuous abandoned channel-fill features are absent in both SNESIM and DEESSE outputs.

22

Similar to previous cases, considerable time was required for effective parameterization. For DEESSE, the chosen values for SR (Search Radius) and DTR (Deactivation threshold radius) gave rise to patchy and chaotic geobodies, and resulted in proportions of floodplain facies in the sand-fairway region that do not honour the probability grid (i.e., floodplain deposits represent over 10% of this region; cf. Fig. 4).

Vertical sections display sandbody compartmentalized by channel-fill deposits. The point-bar fining-upward trend is not typically evident in either SNESIM or DEESSE outputs. The lack of a clear differentiation between different point-bar bodies makes it difficult to ascertain the reproduction of downstream facies trends within them. Overall, the geobodies bear little resemblance to the patterns present in the TIs.
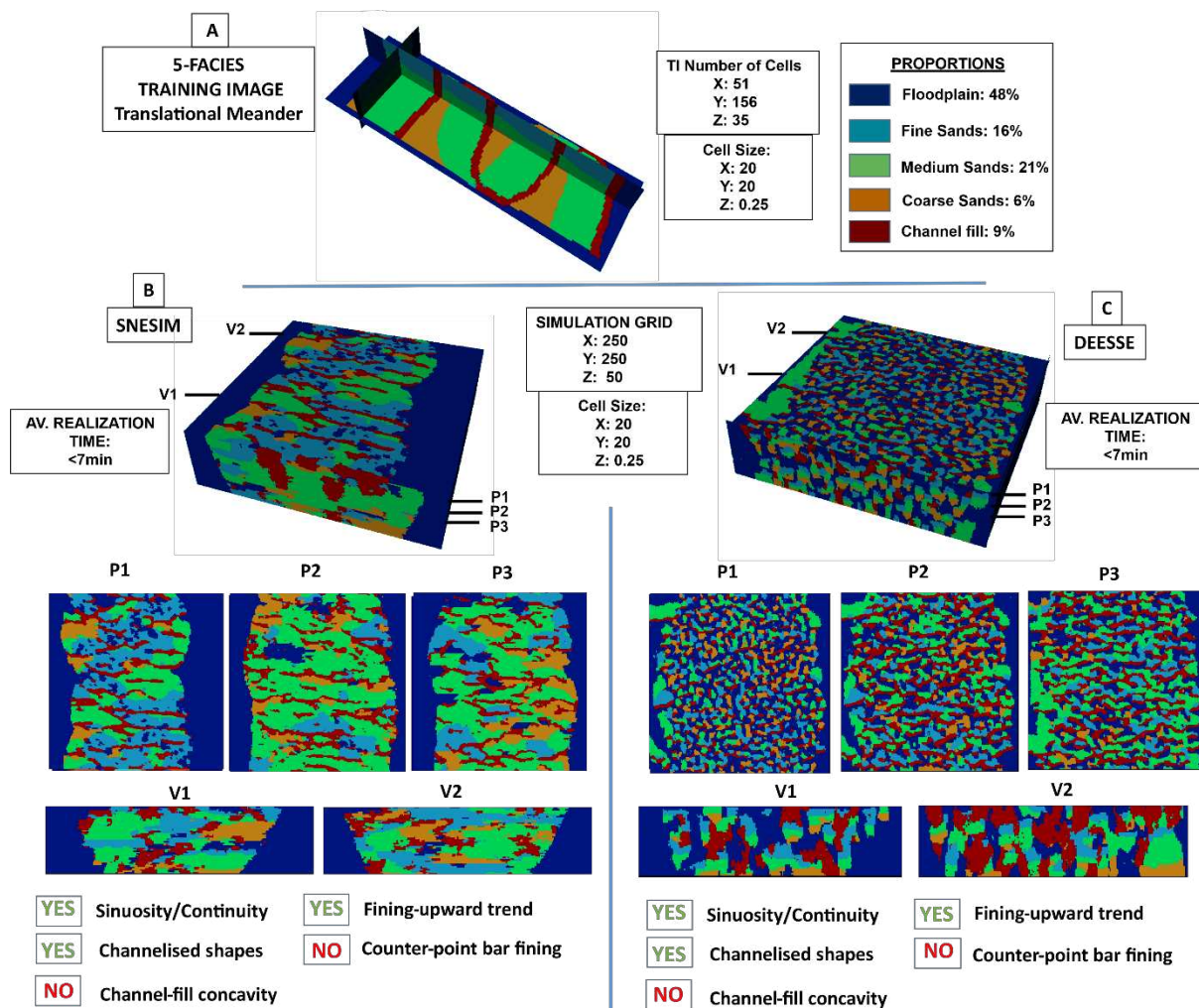
Figure 11: Representative simulation results for the 5-facies training image for meander belts with downstream translating meanders (case 6). (A) Employed training image. Number of cells, cell size and proportions are indicated. Simulations performed for SNESIM (B) and DEESSE (C) are presented as block models in perspective view, together with 3 plan-view sections (P1, P2 and P3) and 2 vertical sections (V1 and V2) for each. A summary of the number of cells for the simulation grid is reported between part B and C. Below the vertical sections, a qualitative assessment of the realizations is presented for each simulation method.

5. DISCUSSION

The intent of this research was not to test modelling algorithms through a systematic assessment of their performance, with the aim to provide definitive guidance on parameter tuning; work of this type already exists, as applied to both SNESIM and DEESSE (Liu et al., 2004; Meerschman et al., 2013). Rather, we determined the ability of these MPS modelling methods to reproduce the types of geological architectures that are characteristic of successions deposited by meandering fluvial systems, since this is a geological context to which MPS is often applied (Rojas et al., 2012; Manchuk et al., 2011; Manchuk and Deutsch, 2012; Arnold et al., 2019), but which is characterized by heterogeneities that are intrinsically non-stationary (Nanson and Page, 1983; Thomas et al., 1987; Alpak and Barton, 2014; Russell et al., 2019). Concurrently, this work:

(i) provides a test of the suitability of the proposed forward stratigraphic modelling software (PB-SAND; Yan et al., 2017, 2019, 2020; Colombera et al., 2018) as a training-image creator, which allows producing trends that would not be readily generated using general-purpose tools (e.g., Maharaja, 2008);

(ii) outlines a workflow that is applicable in cases where a framework exists of the larger-scale architecture of a fluvial succession, consisting of the distribution of large-scale channelized geobodies representing channel belts or valley fills, within which sedimentary heterogeneity needs to be predicted; in reservoir-modelling situations, this framework may be established based on outputs of other modelling efforts (e.g., object-based modelling) linked with MPS in a hierarchical fashion, or by defining channelized geobodies recognizable in 3D seismic cubes; in this way, regions of the reservoir volumes can be defined that can be utilized in the same manner as the probability grids adopted to generate the unconditional realizations discussed in this work.

As applied to SNESIM and DEESSE using training images that incorporate 3 facies only (representing point-bar, channel-fill and overbank deposits) and that relate to channel-belt architectures associated with simple meander expansion, the proposed workflows were effectively employed to model the distribution of channel-fill deposits. The resultant simulated outputs reveal the presence and expected distribution of compartments within meander-belt deposits.

Similar results were observed when using 4-facies training images for expansional point bars, where thick accumulations of mud are also simulated within the point-bar compartments. The successful application of training images incorporating 3 and 4 facies are particularly important as these types of simulation are the preferred scenarios for many simulations of fluvial reservoir successions. When feeding a dynamic simulation, these static models will effectively discriminate facies that act as barriers to fluid flow (floodplain, channel-fill and bar-front mud) from more permeable reservoir volumes (point-bar deposits).

By contrast, the application of training images that incorporate 3, 4 and 5 facies relating to channel-belt architectures associated with meander translation returned realizations that contained discontinuous string-shaped channel-fill geobodies arranged perpendicular to the axis of the sand fairway, rather than units that are continuous and sinuous in planform, as was expected. Also, trends incorporated in the training image such as downstream or upward fining do not seem to be well replicated by either SNESIM or DEESSE. This highlights limitations in the application of these codes to reproduction of trends of this type.

The 5-facies simulations were performed for the two different types of training images. Contrary to the 3-facies training images, the aim for this set of model runs was to simulate a scenario where three different types of bar deposits (sands forming reservoir units) can be differentiated from two types of mud-prone units (channel-fill and floodplain facies – typically non-net reservoir). For both SNESIM and DEESSE, the implemented fining-upward trend is recognized in all the realizations, allowing effective differentiation of different vertically stacked, genetically related bars and channel fills. Channelized shapes are also recognized in the vertical section. However, a decrease in sinuosity and continuity of channel-fill deposits has been acknowledged in the horizontal planes. Loops are rarely distinguished, unlike in 3- and 4-facies simulations obtained using the training images related to expansional meanders. Moreover, simulations appear patchy where different types of point-bar facies are populated in sandy compartments. Runtime for these types of simulations were significantly higher than for the 3- and 4-facies simulations. However, all realizations were still generated in less than 10 minutes based on the chosen inputs.

Based on the qualitative criteria of geological realism considered in this work, an algorithm – SNESIM or DEESSE – that performs consistently better cannot be indicated. Rather, the manner in which features incorporated in the training images are reproduced by either algorithm appears to depend on a combination of input parameters, type of architecture being modelled, and number and types of facies considered.

The simulations performed in this research are not associated with a specific physical scale. The size and resolution of the TIs were important factors in the simulations for dictating geological realism and runtime. The relative size of the TI (number of cells) with respect to the relative size of the simulation grid was calibrated to the size of geobodies to be reproduced in the realizations. For example, the reproduction of large-scale patterns requires training images whose size might be close to the size of the simulation grid. Modelled channelized features will tend to be discontinuous in planform if the TI is smaller than the modelling grid. However, if the training image includes small-scale features that must be reproduced in the simulation grid, a larger number of cells is required (Caers and Zhang, 2004). However, the greater the number of cells in the training image, the greater the runtime needed to perform the simulations in both SNESIM and DEESSE. The size of the geobodies is controlled by the number of cells in the training image with respect to the number of cells in the simulation grid.

Differences were observed in runtime when SNESIM and DEESSE needed to handle training images with larger number of cells. An example of the differences can be seen in cases 2 and 5 where DEESSE realizations required significantly longer runtime than those created using SNESIM. In these cases, the input parameters employed initially resulted in runtime that exceeded the established 10 minutes threshold per realization, so a further upscaling was performed to create a coarser TI for use in DEESSE simulations.

The iterative process by which parameters are optimized in order to deliver relatively realistic realizations within the target runtime is time-consuming, and likely represents a barrier to the widespread uptake of this method by geomodellers. On the basis of the experience acquired through this work, some recommendations can be made that can be used to guide modelling practice, as follows:

(i)   Both the Search Mask (SNESIM) and the Search Neighbourhood (DEESSE) should be set to a size that is sufficiently large to allow the algorithm to borrow the required patterns from the training image along horizontal axes. This study always considered search masks and search neighbourhood values that span the number of cells needed to cover the full amplitude of a meander bend (point bar). Working with large 3D training images often results in excessive runtime.

(ii)   To speed up the modelling effort, it is recommended that parameter tuning is initially performed on 2D grids with any given orientation (X, Y or Z).

(iii)   Calibrating the use of the probability grids in DEESSE can be time-consuming. Unlike SNESIM, which only requires the choice of a TAU model, DEESSE demands setting the weight of the probability grid in the simulations, which requires a search radius (SR) and deactivation threshold radius (DTR) to be optimized simultaneously. A recommendation can be made for a calibration of probability grids starting from values of SR and DTR that are relatively high (>10); smaller values for SR and DTR resulted in excessive runtime.

6. CONCLUSIONS

A hierarchical workflow for the application of MPS modelling algorithms (SNESIM and DEESSE) has been tested by modelling sedimentary architectures that are characteristic of high-sinuosity fluvial meandering systems. The hierarchical approach involves the use of 3D training images for 2 different scenarios (associated with fluvial systems development via bar expansion and translation respectively), each incorporating either 3, 4 or 5 facies. Training images were built using a forward stratigraphic model (PB-SAND) partly conditioned on geological-analogue data borrowed from a sedimentological database (FAKTS), together with auxiliary variables that describe facies probability and input parameters to the algorithms that are optimized for delivering realizations in less than 10 minutes on a standard desktop personal computer. The proposed workflow can be employed in real-world reservoir

modelling scenarios through the use of probability grids constrained on seismic geobodies, or through linkage to outputs of object-based modelling.

The comparison between unconditional realization generated using SNESIM and DEESSE enables evaluation of their performance in modelling fluvial successions, assuming a target runtime of up to 10 minutes. Realizations have been assessed qualitatively against (i) the training images, and (ii) known characteristics of sedimentary architectures of high-sinuosity river systems. Analysis of simulation results indicate what geological features of meandering fluvial successions arising from expansional and translational point-bar development are reproduced.

Planform curvilinear and channelized geometries in the cross-section are sometime evident in modelled channel-fill deposits. Furthermore, under certain modelling inputs, modelled sand-prone point-bar facies take the form of compartments that are juxtaposed horizontally and vertically. This modelling set up is applicable to simulate the architecture of meandering reservoir successions requiring prediction of the degree of stratigraphic compartmentalization of effective net reservoir units by mud plugs. Fining-upward trends incorporated in the 5-facies training image for expansional bars are successfully reproduced by both SNESIM and DEESSE. This modelling approach finds application to reservoir models requiring finer-scale petrophysical characterization of point-bar deposits, especially in contexts of enhanced oil recovery. However, for simulations based on training images associated with translational meanders, the desired differentiation of counter-point bar fines and the geometry of channel-fill meander loops were not readily replicated.

Geomodelling workflows that employ MPS simulations recommend use of stationary training images and incorporation of trends by using auxiliary variable maps. This study demonstrates that geological trends that are incorporated in the training image itself (e.g., point-bar fining-upwards) can be reproduced in some circumstances. Moreover, this research highlights the potential value of a comprehensive training-image library for fluvial depositional systems (cf. Pyrcz et al., 2008), from which geomodellers could select training images and associated modelling recipes based on types of heterogeneities that need to be modelled and target runtime.

7. ACKNOWLEDGEMENTS

8. REFERENCES

Arnold, D., Demyanov, V., Rojas, T. and Christie, M., Uncertainty Quantification in Reservoir Prediction: Part 1—Model Realism in History Matching Using Geological Prior Definitions. Mathematical Geosciences, 2019, 51(2), 209-240. https://doi.org/10.1007/s11004-018-9774-6

Bluck, B. J. Sedimentation in the meandering river Endrick. Scottish Journal of Geology, 1971, 7(2), 93–138. https://doi.org/10.1144/sjg07020093

Bridge, J. and Leeder, M. A., Simulation model of alluvial stratigraphy. Sedimentology, 1979, 26(5): 617–644. https://doi.org/10.1111/j.1365-3091.1979.tb00935

Caers, J., Geostatistical reservoir modelling using statistical pattern recognition, Journal of Petroleum Science and Engineering, 2001, 29(3-4): 177–188. https://doi.org/10.1016/S0920-4105(01)00088-2

Caers, J., Petroleum Geostatistics. Society of Petroleum Engineers, 2005.

Caers, J. and Zhang, T., Multiple-point geostatistics: a quantitative vehicle for integrating geologic analogs into multiple reservoir models. In: G. M. Grammer, P. M. Mitch Harris, & G. P. Eberli, eds., Integration of outcrop and modern analogs in reservoir modeling: AAPG Memoir, 2004, 80: 383–394.

Cannon, S., Reservoir Modelling: A practical guide. Wiley Blackwell, 2018.

Chugunova, T.L. and Hu, L.Y., Multiple-point simulations constrained by continuous auxiliary data. Mathematical Geosciences 2008, 40(2): 133–146. https://doi.org/10.1007/s11004-007-9142-4

Colombera, L., Mountney, N.P., and McCaffrey, W.D., A relational database for the digitization of fluvial architecture concepts and example applications. Petroleum. Geoscience, 2012, 18(1): 129. http://dx.doi.org/10.1144/1354-079311-021

Colombera, L., Felletti, F., Mountney, N.P. and McCaffrey, W.D., A database approach for constraining stochastic simulations of the sedimentary heterogeneity of fluvial reservoirs. AAPG Bulletin, 2012, 96(11): 2143–2166. https://doi.org/10.1306/04211211179

Colombera, L., Mountney, N.P. and McCaffrey, W.D., A quantitative approach to fluvial facies models: methods and example results. Sedimentology, 2013, 60(6): 1526–1558. https://doi.org/10.1111/sed.12050

Colombera, L., Mountney, N. P., Russell, C. E., Shiers, M. N., & McCaffrey, W. D. Geometry and compartmentalization of fluvial meander-belt reservoirs at the bar-form scale: Quantitative

insight from outcrop, modern and subsurface analogues. Marine and Petroleum Geology, 2017, 82, 35-55. https://doi.org/10.1016/j.marpetgeo.2017.01.024

Colombera, L., Yan, N., McCormick-Cox, T. and Mountney, N.P., Seismic-driven geocellular modeling of fluvial meander-belt reservoirs using a rule-based method. Marine and Petroleum Geology, 2018, 93, 553–569. https://doi.org/10.1016/j.marpetgeo.2018.03.042

Corbett, P., Hamdi, H. and Gurav, H., Layered fluvial reservoirs with internal fluid cross flow: A well-connected family of well test pressure transient response. Petroleum Geoscience, 2012, 18(2), 219–229. https://doi.org/10.1144/1354-079311-008

Deutsch, C. V., Annealing Techniques Applied to Reservoir Modeling and the Integration of Geological and Engineering (Well Test) Data. PhD thesis, Stanford University, Stanford, CA, 1992.

Deutsch, C. V., and Wang, L., Hierarchical object-based stochastic modeling of fluvial reservoirs: Mathematical Geology, 1996, 28(7): 851–880. https://doi.org/10.1007/BF02066005

Deutsch, C.V. and Journel, A.G., GSLIB. Geostatistical Software Library and User's Guide, 2nd ed. x + 369 pp. + CD-ROM. Oxford, New York: Oxford University Press, 1998. https://doi.org/10.1017/S0016756899531774

De Vries, L., Carrera J., Falivene O., Gratacos O. and Slooten L., Application of multiple point geostatistics to non-stationary images, Mathematical Geoscience, 2009, 41(1), 29–42. https://doi.org/10.1007/s11004-008-9188-y

Farmer, C.L., The generation of stochastic fields of reservoir parameters with specified geostatis-tical distributions, In: Edwards, S., and King, P. R., eds., Mathematics in oil production, Clarendon Press, Oxford, 1988, 235–252.

Guardiano, F.B. and Srivastava, R.M.no, Multivariate geostatistics: beyond bivariate moments. In: Soares, A., ed., Geostatistics: Troia '92, Kluwer Academic Publishers, Dordrecht, 1993, 133–144.

Haldorsen, H. and Damsleth, E., 1990. Stochastic modelling. Journal of Petroleum Technology, v. 42, no. 4, p. 404–412.

Harding A., Strebelle S., Levy M., Thorne, J., Xie, D., Leigh, S., Preece, R. and Scamman, R.: Reservoir Facies Modelling: New Advances in MPS. Quantitative Geology and Geostatistics Geostatistics Banff 2004, 14

Honarkhah & Caers, Stochastic Simulation of Patterns Using Distance-Based Pattern Modeling. Mathematical Geosciences, 2010, 42, 487-517. https://doi.org/10.1007/s11004-010-9276-7

Hovadik, J.M. and Larue, D.K., Static characterization of reservoirs: refining the concepts of connectivity and continuity. Petroleum Geoscience, 2007, 13(3), 195–211. http://dx.doi.org/10.1144/1354-079305-697

Hubbard, S.M., Smith, D.G., Nielsen, H., Leckie, D.A., Fustic, M., Spencer, R.J. and Bloom, L., Seismic geomorphology and sedimentology of a tidally influenced river deposit, Lower Cretaceous Athabasca oil sands, Alberta, Canada. AAPG Bulletin, 2011, 95(7), 1123–1145. https://doi.org/10.1306/12131010111

Ielpi, A. and Ghinassi M., Planform architecture, stratigraphic signature and morphodynamics of an exhumed Jurassic meander plain (Scalby Formation, Yorkshire, UK): Sedimentology, 2014, 61(7), 1923–1960. https://doi.org/10.1111/sed.12122

Jackson, R., Depositional model of point bars in the lower Wabash River. Journal of Sedimentary Research, 1976, 46 (3), 579–594. https://doi.org/10.1306/212F6FF5-2B24-11D7-8648000102C1865D

Journel, A.G., Geostatistics: Roadblocks and challenges, in Soares, A., ed., Geostatistics: Troia '92, Kluwer Academic, Dordrecht, 1993, 213–224. https://doi.org/10.1007/978-94-011-1739-5_18

Journel, A., Combining knowledge from multiple information sources: An alternative to traditional data independence hypotheses: Mathematical Geology, 2002, 34(5), 573–596. https://doi.org/10.1023/A:1016047012594

Journel, A.G. and Zhang, T., The necessity of a multiple-point prior model. Mathematical Geology, 2006, 38(5), 591–610. https://doi.org/10.1007/s11004-006-9031-2

Krishnan, S., Boucher, A. and Journel, A., Evaluating Information Redundancy through the TAU model. Geostatistic Banff, 2004, 1037–1046. https://doi.org/10.1007/978-1-4020-3610-1_108

Liu, Y., Harding, A., Gilbert, R. and Journel, A.G., A Workflow for Multiple-point Geostatistical Simulation. In: Leuangthong O. and Deutsch C.V. (eds) Geostatistics Banff 2004. Quantitative Geology and Geostatistics, Springer, Dordrecht, 2005, 14(25): 245–254. https://doi.org/10.1007/978-1-4020-3610-1_25

Liu, Y., Using the Snesim program for multiple-point statistical simulation. Computers & Geosciences, 2006, 32(10), 1544–1563. https://doi.org/10.1016/j.cageo.2006.02.008

Ma, Y. Zee. Quantitative Geosciences: Data Analytics, Geostatistics, Reservoir Characterization and Modeling. Springer, 2019.

Walker, R.G. and Cant, D.J., Facies models 3. Sandy fluvial systems. In Facies Model. Ed. R.G. Walker, Geoscience Canada, 1979, 3(1): 23–31.

Maharaja, A., Tigenerator: Object-based training image generator. Computers Geosciences 2008, 34 (12): 1753–1761. https://doi.org/10.1016/j.cageo.2007.08.012

Manchuk, J. G., Lyster, S. J. and Deutsch, C. V., A Comparative Study of Simulation Techniques with Multiple Point Statistics: The MPS Beauty Contest. CCG Annual Report, 2011, 13, Paper 107.

Manchuk, J. G. and Deutsch, C. V., Modeling of the McMurray Formation using MPS Tied to Tidal Range. CCG Annual Report, 2012, 14, Paper 108.

Mariethoz, G., Renard, P. and Straubhaar, J., The Direct Sampling method to perform multiple point geostatistical simulations. Water Resources Research, 2010, 46(11): 1–14. https://doi.org/10.1029/2008WR007621

Meerschman E., Pirot G., Mariethoz G., Straubhaar J., Van Meirvenne M. and Renard, P., A practical guide to performing multiple-point statistical simulations with the Direct Sampling algorithm. Computers & Geosciences, 2013, 52(28), 307–324. https://doi.org/10.1016/j.cageo.2012.09.019

Miall, A.D., The Geology of Fluvial Deposits: Sedimentary Facies, Basin Analysis and Petroleum Geology, Springer, 1996.

Miall, D. Stratigraphy: A modern synthesis. Springer, 2016.

Nanson, G.C. and Page, K.J., Lateral accretion of fine-grained concave benches on meandering rivers, in Collinson, J.D. and Lewin, J., eds., Modern and Ancient Fluvial Systems: International Association of Sedimentologists, 1983, Special Publication 6, 133–143. https://doi.org/10.1002/9781444303773.ch10

Omre, H. Stochastic models for reservoir characterization, in Kleppe, J., and Skjaeveland, S. M., eds., Recent advances in improved oil recovery, methods for North Sea Sandstones reservoirs, Norwegian Petroleum Directorate, Stavanger, Norway, 1991.

Pourfard, M., Abdollahifard, M., J., Faez, K., Motamedi, S., A. and Hosseinian T. PCTO-SIM: Multiple-point geostatistical modeling using parallel conditional texture optimization. Computers & Geosciences, 2017, 102, 116-138. https://doi.org/10.1016/j.cageo.2016.12.012

Pyrcz, M.J., Boisvert, J.B. and Deutsch, C.V., A library of training images for fluvial and deepwater reservoirs and associated code. Computers & Geosciences, 2008, 34(5), 542–560. https://doi.org/10.1016/j.cageo.2007.05.015

Pyrcz, M.J., and Deutsch, C.V., Geostatistical Reservoir Modeling. Oxford University Press, 2014. https://doi.org/10.1007/978-94-011-1739-5_12

Ringrose, P. and Bentley, M., Reservoir Model Design: A practitioner´s guide. Springer, 2015.

Remy, N., Boucher, A. and Wu, J., Applied Geostatistics with SGEMS. A user´s guide. Cambridge University Press, 2009. https://doi.org/10.1017/CBO9781139150019

Riou, J., and Hocker C., Practical recommendations for successful application of the MPS facies modelling method. SPE Abu Dhabi, 2015, SPE-177675-MS. https://doi.org/10.2118/177675-MS

Rojas, T., Demyanov, V., Christie, M., Arnold, D., Reducing uncertainty in modelling fluvial reservoirs by using intelligent geological priors. Paper presented at the Ninth Geostatistical Congress, Olso, 2012.

Russell, C.E., Mountney, N.P., Hodgson, D.M. and Colombera, L., A novel approach for prediction of lithological heterogeneity in fluvial point-bar deposits from analysis of meander morphology and scroll-bar pattern. In: Ghinassi, M., Colombera, L., Mountney, N.P. and Reesink, A.J., eds., Fluvial Meanders and their Sedimentary Products in the Rock Record. International Association of Sedimentologists, Special Publication, 2019, 48, 385–418. https://doi.org/10.1002/9781119424437.ch15

Straubhaar, J., Renard, P., Mariethoz, G., Froidevaux, R. and Besson, O., An improved parallel multiple-point algorithm using a list approach. Mathematical Geosciences, 2011, 43(3), 305-328. https://doi.org/10.1007/s11004-011-9328-7

Straubhaar, J., Walgenwitz, A. and Renard, P., Parallel Multiple-point Statistics Algorithm Based on List and Tree Structures. Mathematical Geoscience, 2013, 45(2), 131–147. https://doi.org/10.1007/s11004-012-9437-y

Strebelle, S., Sequential Simulation Drawing Structures from Training Images, Ph.D. thesis, Department of Geological and Environmental Sciences, Stanford University, Stanford, 2000.

Strebelle, S., and Journel, A., Reservoir modeling using multiple-point statistics: Society of Petroleum Engineers Annual Technical Conference and Exhibition, New Orleans, 2001. SPE Paper 71324: 11. https://doi.org/10.2118/71324-MS

Strebelle, S., Conditional simulation of complex geological structures using multiple-point statistics. Mathematical Geology, 2002, 34(1): 1–21. https://doi.org/10.1023/A:1014009426274

Thomas, R.G., Smith, D.G., Wood, J.M., Visser, J., Calverley-Range, E.A. and Koster, E.H., Inclined heterolithic stratification — terminology, description, interpretation and significance. Sedimentary Geology, 1987, 53(2), 123–179. https://doi.org/10.1016/S0037-0738(87)80006-4

Walker, R.G. and Cant, D.J. Facies models 3. Sandy fluvial systems. In Facies Model. Ed R.G. Walker, Geoscience Canada, 1979, 3(1): 23–31.

Wood, J.M., Alluvial architecture of the upper Cretaceous Judith River Formation. Dinosaur Provincial Park. Alberta. Canada. Bulletin of Canadian Petroleum Geology, 1989, 37(2), 169–181. https://doi.org/10.35767/gscpgbull.37.2.169

Xu, W., Tran, T. T., Srivastava, R. M., and Journel, A. G. Integrating seismic data in reservoir modeling: the collocated cokriging alternative. In 67th Annual Technical Conference and Exhibition, Washington, DC, October 1992. Society of Petroleum Engineers. SPE Paper, 24742: 833-842.

Yan N., Mountney N.P., Colombera, L. and Dorrell, R.M., A 3D forward stratigraphic model of fluvial meander-bend evolution for prediction of point-bar lithofacies architecture, Computers and Geosciences, 2017, 105(7): 65–80. https://doi.org/10.1016/j.cageo.2017.04.012

Yan, N., Colombera, L., Mountney, N.P., Dorrell, D.M. Three-dimensional modelling of fluvial point-bar architecture and facies heterogeneity using analogue data and associated analysis of intra-bar static connectivity: application to humid coastal-plain and dryland fluvial systems. In: Ghinassi, M., Colombera, L., Mountney, N.P. and Reesink, A.J., eds., Fluvial Meanders and their Sedimentary Products in the Rock Record. International Association of Sedimentologists, Special Publication, 2019, 48, 475–508. https://doi.org/10.1002/9781119424437.ch18

Yan, N., Colombera, L. and Mountney, N.P. Three-Dimensional Forward Stratigraphic Modelling of the Sedimentary Architecture of Meandering-River Successions in Evolving Half-Graben Rift Basins, Basin Research, 2020, 31(2), 213–404. https://doi.org/10.1111/bre.12367

Yan, N., Colombera, L. and Mountney, N.P., Controls on fluvial meander-belt thickness and sand distribution: insights from forward stratigraphic modelling, Sedimentology, 2021, in press. https://doi.org/10.1111/sed.12830